

# Dalton Transactions

Accepted Manuscript



This is an *Accepted Manuscript*, which has been through the Royal Society of Chemistry peer review process and has been accepted for publication.

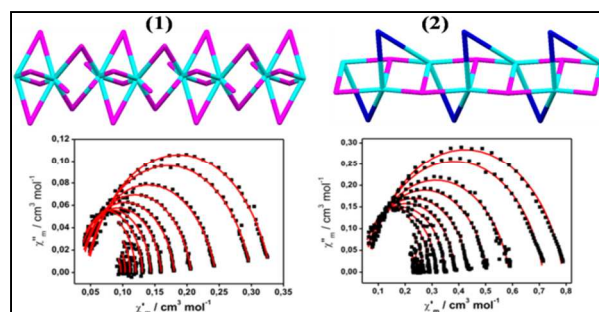
*Accepted Manuscripts* are published online shortly after acceptance, before technical editing, formatting and proof reading. Using this free service, authors can make their results available to the community, in citable form, before we publish the edited article. We will replace this *Accepted Manuscript* with the edited and formatted *Advance Article* as soon as it is available.

You can find more information about *Accepted Manuscripts* in the [Information for Authors](#).

Please note that technical editing may introduce minor changes to the text and/or graphics, which may alter content. The journal's standard [Terms & Conditions](#) and the [Ethical guidelines](#) still apply. In no event shall the Royal Society of Chemistry be held responsible for any errors or omissions in this *Accepted Manuscript* or any consequences arising from the use of any information it contains.

**Graphical Abstract****Neodymium 1D systems: targeting new sources for field-induced slow magnetization relaxation**

Amanpreet Kaur Jassal<sup>a</sup>, Núria Aliaga-Alcalde<sup>b\*</sup>, Montserrat Corbella<sup>c\*</sup>, Daniel Aravena,<sup>d</sup> Eliseo Ruiz<sup>e\*</sup> and Geeta Hundal<sup>a\*</sup>



Two non-isostructural homometallic 1D Neodymium species displaying field-induced slow magnetization relaxations are presented together with theoretical studies. It is established that both systems are better described as organized 1D single molecule magnets (SMMs).

## Neodymium 1D systems: targeting new sources for field-induced slow magnetization relaxation

Cite this: DOI: 10.1039/x0xx00000x

Amanpreet Kaur Jassal,<sup>a</sup> Núria Aliaga-Alcalde,<sup>b\*</sup> Montserrat Corbella,<sup>c\*</sup> Daniel Aravena,<sup>d</sup> Eliseo Ruiz<sup>e\*</sup>, and Geeta Hundal<sup>a\*</sup>

Received 00th January 20xx,  
Accepted 00th January 20xx

DOI: 10.1039/x0xx00000x

www.rsc.org/

**Two non-isostructural homometallic 1D Neodymium species displaying field-induced slow magnetization relaxations are presented together with theoretical studies. It is established that both systems are better described as organized 1D single molecule magnets (SMMs). Studies show a great potential of Nd<sup>III</sup> ions to provide homometallic chains with slow magnetic relaxation.**

Single molecule magnets (SMMs) and single chain magnets (SCMs) stand for 0D and 1D coordination compounds that present slow relaxation of the magnetization and magnetic hysteresis at low temperatures.<sup>1</sup> SMM behavior arises from the combination of large ground-state spin  $S$  and zero-field splitting parameter  $D$  in isolated anisotropic compounds (mono- or polynuclear systems); the slow magnetic relaxation<sup>2</sup> in SCMs however, appears from the magnetic interactions between anisotropic repeating units along well-isolated single chains.<sup>3</sup> Particular ratios between anisotropy and exchange interactions among the metallic centers in the chains, allow the existence of SCM behavior.<sup>4</sup> The interesting link between SMMs and SCMs still deserves further theoretical investigation because the 1D organization of SCMs can induce a significant increase in the energy barrier for the reversal of the magnetization,<sup>5</sup> this being the original motivation for the construction of SCMs.<sup>6</sup>

So far, many of the SCMs reported in the literature are derived from  $3d$  ions,<sup>7</sup> mixed  $3d-4f$  ions<sup>8</sup> or pre-formed bridged  $3d$  SMMs.<sup>9</sup> Much recently, homometallic  $4f$  SCMs<sup>10</sup> have been presented with special interest, toward the creation of new magnetic materials,<sup>11</sup> due to the large anisotropic values of lanthanide carriers (mainly because of their strong spin-orbit contributions) and their moderate magnetic exchange couplings.<sup>12</sup> Everything considered, homometallic  $4f$  SCMs deserve further experimental and theoretical studies. Hitherto, Dy<sup>III</sup>, Tb<sup>III</sup>, Er<sup>III</sup> and Ho<sup>III</sup> ions have been primarily employed<sup>13</sup> but further understanding of the field requires a look on other Ln<sup>III</sup> ions as well, for e.g. Nd<sup>III</sup> presented here. Nd<sup>III</sup> coordination compounds (0D or 1D) have been mostly studied because of their luminescent properties at the near-IR region<sup>14</sup> although it has been shown that few mononuclear Nd<sup>III</sup> systems behave as SMMs.<sup>15</sup>

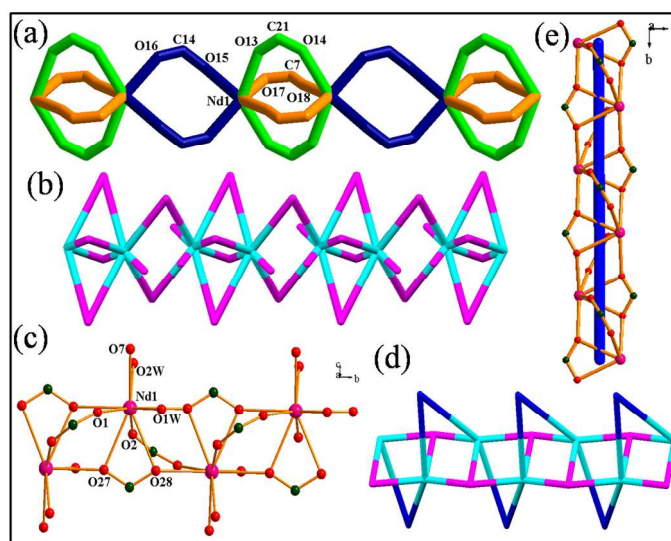


**Fig. 1** (a) L1 bridged paddlewheel dimeric units (green and orange color) further bridged by L1 (blue color), forming linear tapes along  $a$  axis, in **1**. (b)  $[1\ 0\ 0]$  chains of **1** with 2-connected uninodal net. (c) ball-n-stick representation showing coordination environment around Nd<sup>III</sup> in **2**. (d) Acetate bridged ladder along  $[0\ 1\ 0]$  with L2 bridged zig-zag railing in **2**. (e) Helical chain of **2** along the  $b$  axis. Terminally bonded ligands are not shown in d and e.

Now, we report two new non-isostructural Nd<sup>III</sup> chains, compounds **1** and **2**, containing 3,5- and 2,4-dinitrobenzoic acids, L1 and L2, respectively. Despite two different arrangements (different coordination numbers, geometry and distances among Nd<sup>III</sup> ions, Fig. 1) both systems, **1** and **2**, display field induced slow magnetization relaxations, pointing out the rich versatility yet unexplored of 1D Nd<sup>III</sup> systems in the field of molecular magnetism. Recently, Arauzo *et al.*<sup>16</sup> accomplished the first reported Nd<sup>III</sup> homometallic chain that presents field dependence relaxation of the magnetization by the use of cyanoacetate ligands (system differs crystallographically from the two presented in this work). Here, we extend such family by the addition of **1** and **2** and provide theoretical proof disclosing the

relevance of dipolar interactions in front of  $\text{Nd}^{\text{III}} \cdots \text{Nd}^{\text{III}}$  exchange interactions and therefore, implying that at least **1** and **2** should be better described as organized 1D SMMs.

Compound **1**,  $\{[\text{Nd}(\mu_2\text{-L1})_3(\text{H}_2\text{O})_2]\cdot\text{C}_2\text{H}_3\text{N}\}_n$ , was achieved by mixing  $\text{Nd}(\text{NO}_3)_2\cdot 6\text{H}_2\text{O}$  with (**L1**) at room temperature meanwhile compound **2**,  $[\text{Nd}(\mu_2\text{-L2})(\text{L2})(\text{CH}_3\text{COO})(\text{H}_2\text{O})_2]_n$ , was attained after the hydrothermal reaction at 120 °C of  $\text{Nd}(\text{CH}_3\text{COO})_3\cdot\text{H}_2\text{O}$  with (**L2**). Compound **1** is centrosymmetric where geometry around the  $\text{Nd}^{\text{III}}$  ion is bicapped trigonal prismatic with six sites occupied by carboxylate oxygens of **L1** and the remaining two sites by  $\text{H}_2\text{O}$  molecules. Four carboxylate groups from four centrosymmetric **L1** ligands coordinate two  $\text{Nd}^{\text{III}}$  ions, in a  $\mu_2\text{-}\kappa^2, \eta^1:\eta^1$  mode (mode I), with *syn-syn* and *syn-anti* conformation to form paddle wheel type centrosymmetric dimers (Fig. 1a). The successive dimeric units are further bridged by two more centrosymmetric **L1** ligands, again in mode I, with *syn-syn* conformation. The dihedral angles between two Nd-OCO planes in the dimer with Nd-OCO plane in this bridging link are  $45.28(5)^\circ$  and  $46.38(3)^\circ$ , forming twisted ribbons (Fig. 1a) parallel to *a* axis. The two intrachain  $\text{Nd} \cdots \text{Nd}$  distances are 4.267 (8) Å and 5.348(7) Å, respectively. Among chains, the shortest  $\text{Nd} \cdots \text{Nd}$  distance is above 12.6 Å. From a topological perspective, this structure consists of chains [1 0 0] with a 2-connected uninodal net (Fig. 1b).

Compound **2** belongs to chiral space group  $P2_1$  and shows two similar but crystallographically independent molecules in the unit cell (Only one of them has been discussed here and shown in the Fig. 1). In each one of them  $\text{Nd}^{\text{III}}$  is nine coordinated (Fig. 1c), in a trigonal prismatic tricapped geometry. Three sites are occupied by the acetate ions binding in a  $(\mu_2\text{-}\kappa^3, \eta^1:\eta^2)$  mode (mode II), with a *syn-syn* conformation forming a ladder type architecture. Two  $\text{H}_2\text{O}$  molecules and one **L2** ligand are coordinating terminally whereas the second **L2**, in mode I, and *syn-syn* conformation, further links this ladder forming a spiral railing around this ladder (dihedral angle between metal-acetate plane and Nd-OCO-L2 plane is  $89.74(9)^\circ$ ) (Fig. 1d). The resultant 1D polymer is a left handed helical chain about the *b* axis (Fig. 1e). Finally, intermolecular interactions between  $\text{Nd} \cdots \text{Nd}$  go over 7.7 Å. The average Nd-O bond lengths, 2.4291(17) Å and 2.498 (3) Å for compounds **1** and **2** respectively, are comparable to those reported earlier for other  $\text{Nd}^{\text{III}}$ -O complexes.<sup>14</sup> (See Fig. S1-S8, Table S1-S5, ESI for details on X-ray structures).

The magnetic behavior of compounds **1** and **2** was studied by means of magnetic susceptibility experiments in the range of temperatures of 1.8-300 K applying 0.5 and 0.3 T dc fields, respectively. As shown in Fig. 2, the room temperature  $\chi_M T$  values of **1** and **2** are 1.73 and  $1.69 \text{ cm}^3 \text{ K mol}^{-1}$ , in that order, which are only slightly higher than the expected value for an isolated  $\text{Nd}^{\text{III}}$  ion of  $1.64 \text{ cm}^3 \text{ K mol}^{-1}$  (ground level  $^4I_{9/2}$ )<sup>17</sup> pointing out that the magnetic exchange interactions among the  $\text{Nd}^{\text{III}}$  centers, for both chains, should be rather weak or negligible. Upon cooling, the  $\chi_M T$  values of both compounds, **1** and **2** decrease gradually, reaching the values of 0.52 and  $0.79 \text{ cm}^3 \text{ K mol}^{-1}$  at the lowest temperatures, in that order. The magnetization curves of **1** and **2** measured at 2.0 K are similar (insets Fig. 2), showing a gradual increase from the lowest to the highest fields with the absence of plateau in both cases. Maximum values of 1.2 and  $1.5 \mu_B$  were found for **1** and **2**, respectively, where the unsaturated magnetization suggests the presence of magnetic anisotropy and/or the presence of low-lying excited states that might be populated when a field is applied.<sup>18</sup>

In both systems, such magnetic response could be explained by the facts that: a) the  $M_J$  sublevels could be split by the crystal field in the  $\text{Nd}^{\text{III}}$  centres where, on cooling the excited  $M_J$

sublevels, should be progressively depopulated.<sup>19</sup> and/or b) the magnetic exchange interaction/s among neighbor metal ions in the chain. Compounds **1** and **2** present both exclusively  $\text{Nd}^{\text{III}}$  ions attached by carboxylate bridges with *syn-syn* and/or *syn-anti* conformations that could provide antiferro- or weak antiferro/ferro-magnetic exchanges, a part from the contributions of the alkoxy groups in the case of **2**.<sup>20,21</sup> From an experimental point of view, it is not trivial to determine the relative nature and strength of the exchange contribution/s, as equally difficult is the analysis of the crystal field role of the ions in the net magnetic behavior.<sup>22</sup> The correct interpretation of these parameters and their effects requires theoretical studies, as key analyses for the proper description of the magnetic behavior. Hence, to further investigate the interplay of local crystal field and coupling effects for compounds **1** and **2**, CASSCF+RASSI calculations were performed, as implemented in the MOLCAS 7.8 software package.<sup>23</sup>

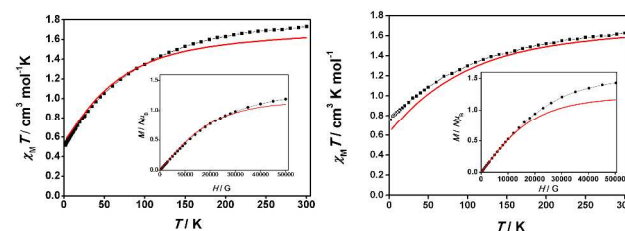


**Fig. 2** (left) Plot of  $\chi_M T$  vs  $T$  for **1** (black dots correspond to the experimental measures while red line is the simulated curve using the CASSCF results for a truncated model chain using the POLY\_ANISO code, see Computational Studies section). Inset:  $M/N\mu_B$  vs  $H$  at 2 K. (right) Plot of  $\chi_M T$  vs  $T$  for **2**. Inset:  $M/N\mu_B$  vs  $H$  at 2 K.

The CASSCF+RASSI (or CASSCF+QDPT) approach is especially appropriate to handle the magnetic anisotropy in lanthanide systems,<sup>24,25</sup> as it considers the multi reference nature of the low-lying electronic energy spectrum of lanthanide-based compounds and includes the state mixing due to spin-orbit coupling, which is crucial for SMM/SCM properties. Starting from the X-ray diffraction structures, the molecular chains were truncated to monomeric models, where the immediate coordination environment of the  $\text{Nd}^{\text{III}}$  ions was preserved. Neighbor  $\text{Nd}^{\text{III}}$  ions were modeled as  $\text{La}^{\text{III}}$  *ab initio* model potentials (truncated geometries are presented in ESI, Fig. S9). 35 quartet and 112 doublet roots were considered for the CASSCF step, while the employed ANO basis set had the following contraction patterns: Nd [9s8p6d4f3g2h]; O [4s3p1d]; N [4s3p21d]; C [3s2p]; H [2s]. Spin Hamiltonian parameters (such as *g*-factors) were calculated through the SINGLE\_ANISO program.<sup>26</sup>

The calculated values collected in Table 1 show a large anisotropy for the two systems, **1** and **2**, with a relatively low energy for the first excited state ( $77.8 \text{ cm}^{-1}$  and  $87.3 \text{ cm}^{-1}$  for **1** and **2**, respectively). In Fig. 2, calculated magnetization and susceptibility curves are represented together with the experimental ones, with reasonable agreement in both cases, assuming that the exchange interaction is negligible<sup>24</sup> and only the dipolar term is taken into account (performed with the POLY\_ANISO code).<sup>27</sup> Verification of the shape of the curve remaining constant was performed by increasing the number of  $\text{Nd}^{\text{III}}$  centers (from 2 to 10 centers) in the truncated chain structure employed in the simulation. This assumption was also previously shown valid in  $\text{Ho}^{\text{III}}$  compounds.<sup>28</sup> The largest  $\chi_M T$  value at low temperature for **2** in comparison with **1** is due to the larger magnetic moment of the ground state for the system **2** as reflected in the  $g_z$  values shown in Table 1.

**Table 1** Calculated CASSCF+RASSI energies ( $\text{cm}^{-1}$ ) and  $g$ -factors for the five lowest Kramers' doublets for the truncated models of compounds **1** and **2**.

	<b>1</b>				<b>2</b>			
	Energy	$g_z$	$g_y$	$g_x$	Energy	$g_z$	$g_y$	$g_x$
1	0.0	3.514	2.012	1.021	0.0	4.122	1.730	0.622
2	77.8	0.100	1.842	3.075	87.3	3.035	1.504	0.971
3	171.8	4.037	1.130	0.106	188.0	4.415	0.862	0.297
4	225.6	0.967	2.319	3.255	285.0	0.197	1.902	2.837
5	259.3	3.615	1.973	1.294	325.8	0.619	2.881	3.474

In addition, to investigate the magnetization dynamics, the temperature dependent alternating current (ac) susceptibility data for **1** and **2** were collected with and without applied dc fields. In the absence of a dc field, neither peaks nor frequency dependence were observed for the in-phase ( $\chi_M'$ ) and out-of-phase ( $\chi_M''$ ) signals for any of the compounds under study. However, when a small dc field was applied, frequency dependence was observed for both systems due to the full or partial suppression of the quantum tunneling relaxation of the magnetization. To find the optimal dc field, parallel experiments for **1** and **2** were performed at 2.0 K when applying dc fields in the range of 0-0.3 T (Fig. S10) and 0-0.4 T (Fig. S11), respectively. As a result, 0.20 T and 0.35 T dc fields (those that induce the slowest relaxation) were chosen as the optimum fields for **1** and **2**, in that order. Afterward, we performed dynamic ac magnetic susceptibility measurements for **1** and **2** (applying the corresponding dc magnetic field) as a function of temperature. The ac signals become frequency-dependent below approx. 7.0 K for **1** and **2** and maxima peaks were observed around 5.0 K in both cases as well (Fig. 3). Therefore, both systems display typical SMM behaviors, in agreement with the theoretical calculations, where the relatively large transversal components of the magnetic moment ( $g_x$  and  $g_y$  in Table 1) are consistent with the lack of slow relaxation at zero-field.

The ac susceptibility data plotted as Cole-Cole plots between 1.8 and 7.0 K (used T (K): 1.8, 2.0, 2.5, 3.0, 3.5, 4.0, 4.5, 5.0, 5.5, 6.0, 6.5 and 7.0) for the two compounds show relatively symmetrical shapes (Fig. 4 top). In both cases, the fitting of the corresponding Cole-Cole data were performed with the CC-FIT program.<sup>29</sup> From here it was found that the  $\alpha$  parameters were always below 0.18 for **1** and 0.15 for **2**, in that order, indicating all together the existence in both systems of a single magnetization relaxation process with a narrow distribution of relaxation times.<sup>30</sup>

The fitting also provided the relaxation times,  $\tau$ 's, for **1** and **2** at each temperature. By means of the Arrhenius law, the energy barrier defined as  $U_{\text{eff}}/K$  and the pre-exponential factor for the Arrhenius law ( $\tau_0$ ) were obtained (Fig. 4 bottom). This way, compound **1** show values of  $U_{\text{eff}}/K = 27$  K ( $19 \text{ cm}^{-1}$ ) and  $\tau_0 = 4.1 \cdot 10^{-7}$  s and compound **2** of  $U_{\text{eff}}/K = 29$  K ( $20 \text{ cm}^{-1}$ ) and a  $\tau_0 = 3.1 \cdot 10^{-7}$  s, in that order. Overall, these two non-isostructural, homometallic 1D systems display similar magnetic behavior which lies between the expected range for a SCM, comparable also to other 4f- and 3d-4f-SCMs and SMMs in the literature.<sup>31</sup>

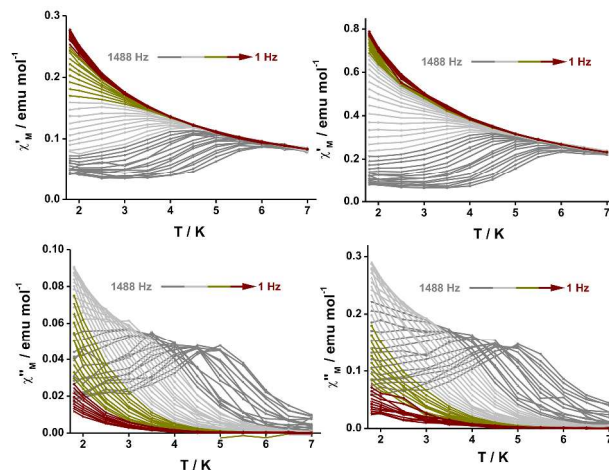


**Fig. 3** In-phase (top) and out-of-phase susceptibilities (bottom) of compounds **1** (left) and **2** (right) applying an external dc magnetic field and frequencies from 1 Hz to 1488 Hz (see list of frequencies in the supp. Inf.)

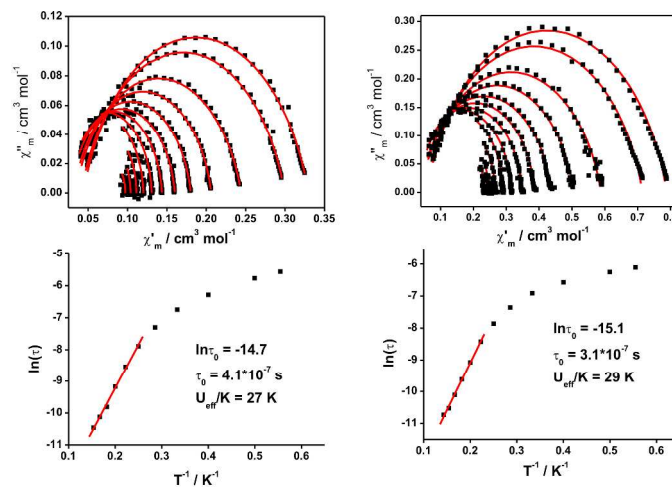


**Fig. 4** (Top) Cole-Cole plots for **1** (left) and **2** (right) obtained using the ac susceptibility data applying an external dc magnetic field. (Bottom) The  $\ln \tau$  vs.  $T^{-1}$  plots of **1** (left) and **2** (right). The solid lines are best fits in all the plots.

In summary, we have described two different 1D  $\text{Nd}^{\text{III}}$  systems, compounds **1** and **2**, that present slow relaxation of the magnetization by applying an external dc field, with  $U_{\text{eff}}/K$  values comparable to other lanthanides SMM and SCM in the literature. These two compounds are crystallographically non-isostructural, fact that emphasizes the unexplored possibilities of  $\text{Nd}^{\text{III}}$  systems in the field of molecular magnetism and at the same time, our theoretical studies show that the  $\text{Nd} \cdots \text{Nd}$  exchange interactions in the two systems are negligible, been the dipolar contribution the main factor to explain the magnetic performance, behaving both as organized 1D SMMs.

† This article is dedicated to Late Professor Maninder Singh Hundal.

‡ Electronic Supplementary Information (ESI) available: [X-Ray experimental details, tables of selected bond lengths ( $\text{\AA}$ ) and angles ( $^\circ$ ), Important Hydrogen bond distances ( $\text{\AA}$ ) and angles ( $^\circ$ ), detail of Thermo

gravimetric analysis and IR spectroscopy, graphs of Magnetic properties, CCDC no. **1051022** and **1051023**.

A.K. Jassal thanks Department of Science and Technology for INSPIRE fellowship. G.H. thanks University Grants Commission (India) for research grant under UPE (University with potential for excellence) scheme for GNDU, for financial assistance. The research reported here was supported by the Spanish Ministerio de Economía y Competitividad (grants CTQ2011-23862-C02-01, CTQ2012-32247 and CTQ2012-30662). E.R. thanks Generalitat de Catalunya for an ICREA Academia fellowship. D.A. thanks CONICYT+PAI "Concurso nacional de apoyo al retorno de investigadores/as desde el extranjero, convocatoria 2014 82140014". The authors thankfully acknowledge the computer resources, technical expertise and assistance provided by the CIESCA

## Notes and references

<sup>a</sup>Department of Chemistry, Centre of Advance Studies-II, Guru Nanak Dev University, Amritsar, Punjab, India.

<sup>b</sup>ICREA (Institut de Recerca i Estudis Avançats) – ICMAB-CSIC (Institut de Ciència de Materials de Barcelona), Campus UAB, 08193 Bellaterra, Spain.

<sup>c</sup>Departament de Química Inorgànica and Institut de Nanociència i Nanotecnologia, Universitat de Barcelona, Martí i Franquès 1-11, 08028 Barcelona, Spain.

<sup>d</sup>Departamento de Química de los Materiales, Facultad de Química y Biología, Universidad de Santiago de Chile (USACH), Casilla 40, Correo 33, Chile

<sup>e</sup>Departament de Química Inorgànica and Institut de Recerca de Química Teòrica i Computacional, Universitat de Barcelona, Diagonal 645, 08028 Barcelona, Spain.

- (a) R. Gheorghe, A. M. Madalan, J.-P. Costes, W. Wernsdorfer, M. Andruh, *Dalton Trans.*, 2010, **39**, 4734-4736. (b) Y. Wang, X.-L. Li, T.-W. Wang, Y. Song, X.-Z. You, *Inorg. Chem.*, 2010, **49**, 969-976. (c) L. Bogani, C. Sangregorio, R. Sessoli, D. Gatteschi, *Angew. Chem., Int. Ed.*, 2005, **44**, 5817-5821. (d) K. Bernot, L. Bogani, A. Caneschi, D. Gatteschi, R. Sessoli, *J. Am. Chem. Soc.*, 2006, **128**, 7947-7956. (e) X. Wang, X. Bao, P. Xu and L. Li, *Eur. J. Inorg. Chem.*, 2011, 3586-3591.
- A. Caneschi, D. Gatteschi, N. Lalio, C. Sangregorio, R. Sessoli, G. Venturi, A. Vindigni, A. Rettori, M. G. Pini, M. A. Novak, *Angew. Chem., Int. Ed.*, 2001, **40**, 1760-1763.
- (a) G. Aromí and E. K. Brechin, *Struct. Bonding*, 2006, **122**, 1-67. (b) D. Gatteschi, R. Sessoli, J. Villain, *Molecular Nanomagnets*, Oxford University Press, Oxford, 2006.
- J. Lajzerowicz, J. J. Niez *J. Phys. Lett.*, 1979, **40**, L165-L169.
- (a) H.-L. Suna, Z.-M. Wang, S. Gao, *Coord. Chem. Rev.*, 2010, **254**, 1081-1100. (b) R. Sessoli, A. K. Powell, *Coord. Chem. Rev.*, 2009, **253**, 2328-2341. (c) L. Bogani, A. Vindigni, R. Sessolia, D. Gatteschi, *J. Mater. Chem.*, 2008, **18**, 4750-4758. (d) R. Inglis, L. F. Jones, C. J. Milios, S. Datta, A. Collins, S. Parsons, W. Wernsdorfer, S. Hill, S. Perlepes, S. Piligkos, E. K. Brechin, *Dalton Trans.*, 2009, 3403-3412. (e) C. Milios, S. Piligkos, E. K. Brechin, *Dalton Trans.*, 2008, 1809-1817. (f) A. M. Ako, V. Mereacre, R. Clerac, W. Wernsdorfer, I. J. Hewitt, C. E. Anson, A. K. Powell, *Chem. Commun.*, 2009, 544-546.
- (a) R. Clérac, H. Miyasaka, M. Yamashita, C. Coulon *J. Am. Chem. Soc.*, 2002, **124**, 12837-12844. (b) W.-X. Zhang, R. Ishikawa, B. Breedlove, M. Yamashita, *RSC Adv.*, 2013, **3**, 3772-3798.
- (a) X. Y. Duan, X. Cheng, J. G. Lin, S. Q. Zang, Y. Z. Li, C. J. Zhu, Q. J. Meng, *Cryst. Eng. Comm.*, 2008, **10**, 706-714. (b) S. Su, C. Qin, S. Song, Z. Guo, R. Deng, W. Chen, X. Song, S. Wang, G. Li, H. Zhang, *Cryst. Eng. Comm.*, 2011, **13**, 6057-6064.
- (a) D. Visinescu, A. M. Madalan, M. Andruh, C. Duhayon, J.-P. Sutter, L. Ungur, W. Van den Heuvel, L. F. Chibotaru, *Chem.-Eur. J.*, 2009, **15**, 11808-11814. (b) R. Gheorghe, A. M. Madalan, J.-P. Costes, W. Wernsdorfer, M. Andruh, *Dalton Trans.*, 2010, **39**, 4734-4736.
- H.B. Xu, B.W. Wang, F. Pan, Z.M. Wang, S. Gao, *Angew. Chem., Int. Ed.*, 2007, **46**, 7388-7392.
- F. Luo, Z.-w. Liao, Y.-m. Song, H.-x. Huang, X.-Z. Tian, G.-M. Sun, Y. Zhu, Z.-Z. Yuan, M.-B. Luo, S.-J. Liu, W.-Y. Xu, X.-F. Feng, *Dalton Trans.*, 2011, **40**, 12651-12655.
- Y.-G. Huang, X.-T. Wang, F.-L. Jiang, S. Gao, M.-Y. Wy, Q. Gao, W. Wei, M.-C. Hong, *Chem. Eur. J.* **2008**, **14**, 10340-10347.
- (a) H. Ke, G.-F. Xu, Y.-N. Guo, P. Gamez, C. M. Beavers, S. J. Teat, J. Tang, *Chem. Commun.*, 2010, **46**, 6057-6059. (b) R. Sessoli, A. K. Powell, *Coord. Chem. Rev.*, 2009, **253**, 2328-2341. (c) S. K. Langley, B. Moubarak, C. M. Forsyth, I. A. Gass, K. S. Murray, *Dalton Trans.*, 2010, **39**, 1705-1708 (d) X. Wang, X. Bao, P. Xu, L. Li *Eur. J. Inorg. Chem.* 2011, 3586-3591.
- (a) N. Ishikawa, M. Sugita, W. Wernsdorfer, *J. Am. Chem. Soc.*, 2005, **127**, 3650-3651; (b) N. Ishikawa, M. Sugita, W. Wernsdorfer, *Angew. Chem. Int. Ed.*, 2005, **44**, 2931-2935; (c) S. Takamatsu, T. Ishikawa, S.-y. Koshihara, N. Ishikawa, *Inorg. Chem.*, 2007, **46**, 7250-7252.
- (a) S. Chen, R.-Q. Fan, C.-F. Sun, P. Wang, Y.-L. Yang, Q. Su, Y. Mu, *Cryst. Growth Des.* 2012, **12**, 1337-1346 (b) F. Dai, P. Cui, F. Ye, D. Sun *Cryst. Growth Des.*, 2010, **10**, 1474-1477.
- (a) Y.-L. Wang, Y.-L. Jiang, Z.-J. Xiahou, J.-H. Fu, Q.-Y. Liu, *Dalton Trans.*, 2012, **41**, 11428-11437. (b) J. Gu, Z. Gao, Y. Tang, *Cryst. Growth Des.* 2012, **12**, 3312-3323.
- A. Arauzo, A. Lazarescu, S. Shova, E. Bartolomé, R. Cases, J. Luzón, J. Bartolomé, C. Turta, *Dalton Trans.*, 2014, **43**, 12342-12356.
- J. Rossat-Mignod, *Systematics and the Properties of the Lanthanides NATO ASI Series*, 1983, **109**, 255-310.
- D. Zeng, M. Ren, S.-S. Bao, L. Li, L.-M. Zheng, *Chem. Commun.*, 2014, **50**, 8356-8359.
- D. T. Thielemann, M. Klinger, T. J. A. Wolf, Y. Lan, W. Wernsdorfer, M. Busse, P. W. Roesky, A.-N. Unterreiner, A. K. Powell, P. C. Junk, G. B. Deacon, *Inorg. Chem.*, 2011, **50**, 11990-12000.
- H. Arora, R. Mukherjee, *New J. Chem.*, 2010, **34**, 2357-2365.
- F. J. Kettle, V. A. Milway, F. Tuna, R. Valiente, L. H. Thomas, W. Wernsdorfer, S. T. Ochsenbein, M. Murrie, *Inorg. Chem.*, 2014, **53**, 8970-8978.
- T. Hamamatsu, K. Yabe, M. Towatari, S. Osa, N. Matsumoto, N. Re, A. Pochaba, h. Mrozinski, J.-L. Gallani, A. Barla, P. Imperia, C. Paulsen, J.-P. Kappler, *Inorg. Chem.*, 2007, **46**, 4458-4468.
- F. Aquilante, L. De Vico, N. Ferré, G. Ghigo, P.-A. Malmqvist, P. Neogrády, T. B. Pedersen, M. Pitoňák, M. Reiher, M., B. O. Roos, B. O., L. Serrano-Andrés, M. Urban, V. Veryazov, R. Lindh, *J. Comput. Chem.*, 2010, **31**, 224-247.
- D. Aravena, E. Ruiz, *Inorg. Chem.*, 2013, **52**, 13770-13778.
- S. Gómez-Coca, D. Aravena, R. Morales, E. Ruiz, *Coord. Chem. Rev.*, 2015, **289-290**, 379-392.
- L. F. Chibotaru, L. Ungur, *J. Chem. Phys.* 2012, **137**, 064112-064122.
- L. F. Chibotaru, L. Ungur, A. Soncini *Angew. Chem. Int. Ed.* 2008, **47**, 4126-4129.
- J. D. Leng, J. L. Liu, W. Q. Lin, S. Gomez-Coca, D. Aravena, E. Ruiz and M. L. Tong, *Chem Commun*, 2013, **49**, 9341-9343.
- CC-FIT, Copyright © 2014 Nicholas F. Chilton.
- Y.-N. Guo, G.-F. Xu, Y. Guo and J. Tang, *Dalton Trans.*, 2011, **40**, 9953- 9963.
- (a) M. Menelaou, F. Ouharrou, L. Rodríguez, O. Roubeau, S. J. Teat, N. Aliaga-Alcalde, *Chem. Eur. J.*, 2012, **18**, 11545-11549. (b) M.-X. Yao, Q. Zheng, K. Qian, Y. Song, S. Gao, J.-L. Zuo, *Chem. Eur. J.*, 2013, **19**, 294-303. (c) M. A. Palacios, S. Titos-Padilla, J. Ruiz, J. M. Herrera, S. J. A. Pope, E. K. Brechin, E. Colacio, *Inorg. Chem.*, 2014, **53**, 1465-1474.

Electronic Supplementary Information

# Neodymium 1D systems: targeting new sources for field-induced slow magnetization relaxation

Amanpreet Kaur Jassal<sup>a</sup>, Núria Aliaga-Alcalde<sup>b\*</sup>, Montserrat Corbella<sup>c\*</sup>, Daniel Aravena,<sup>d</sup>  
Eliseo Ruiz<sup>e\*</sup> and Geeta Hundal<sup>a\*</sup>

**Corresponding author. Address:** Department of Chemistry, UGC Centre for Advanced Studies-II, Guru Nanak Dev University, Amritsar 143 005, India.

**E-mail address:** [geetahundal@yahoo.com](mailto:geetahundal@yahoo.com)

Content	Pages
<b>1. Experimental Section</b>	<b>(2-3)</b>
1.1 Physical Measurements	
1.2 Synthesis of $\{[\text{Nd}(\mu_2\text{-L1})_3(\text{H}_2\text{O})_2]\cdot\text{C}_2\text{H}_3\text{N}\}_n$ (1)	
1.3 Synthesis of $[\text{Nd}(\mu_2\text{-L2})(\text{L2})(\text{CH}_3\text{COO})(\text{H}_2\text{O})_2]_n$ (2)	
<b>2. X-ray crystallography</b>	<b>(3-4)</b>
References	
<b>3. Results of X-ray crystallography</b>	<b>(5-16)</b>
3.1 $\{[\text{Nd}(\mu_2\text{-L1})_3(\text{H}_2\text{O})_2]\cdot\text{C}_2\text{H}_3\text{N}\}_n$ (1)	
3.2 $[\text{Nd}(\mu_2\text{-L2})(\text{L2})(\text{CH}_3\text{COO})(\text{H}_2\text{O})_2]_n$ (2)	
<b>4. Thermo gravimetric analysis</b>	<b>(16-17)</b>
<b>5. IR spectroscopy</b>	<b>(17-18)</b>
<b>6. PXRD studies</b>	<b>(18-19)</b>
<b>7. Magnetic study</b>	<b>(20-21)</b>

## 1. Experimental Section

### 1.1 Physical Measurements

All the reagents were commercially available and used as received. The melting points were determined with an electrically heated apparatus. C, H, N elemental analyses were obtained with a CHNS-O analyzer flash-EA-1112 series. The IR spectra of compounds were recorded on Perkin ELMER FTIR spectrometer in the range 4000-400 $\text{cm}^{-1}$ . Thermogravimetric analysis (TGA) data were collected on a NetzschTG-209 instrument. Single crystal structural X-ray diffraction was carried out on a Bruker's Apex-II CCD diffractometer using Mo K $\alpha$  ( $\lambda=0.71069\text{\AA}$ ) at room temperature. The X-ray powder diffraction (XRPD) measurements were recorded on a Rigaku miniflex X-ray diffractometer with Cu K $\alpha$  radiation. Magnetic susceptibility measurements were carried out between 2-300 K in a SQUID Quantum Design Magnetometer, model MPMP at the "Unitat de Mesures Magnètiques (Universitat de Barcelona)". Two different magnetic fields were used for each sample in the range of 1.8 - 300 K of 5000 G for **1** and 3000 G for **2**, respectively. Pascal's constants were used to estimate the diamagnetic corrections for the compounds.

### 1.2 Synthesis of $\{[\text{Nd}(\mu_2\text{-L1})_3(\text{H}_2\text{O})_2]\cdot\text{C}_2\text{H}_3\text{N}\}_n$ (**1**)

To a solution of  $\text{Nd}(\text{NO}_3)_2\cdot 6\text{H}_2\text{O}$  (1 mmol, 0.438 g) in 10 mL of water, 2-3 drops of NaOH 0.1 M were added. Then, a suspension of L1 (1 mmol, 0.21 g) in 20 mL of acetonitrile was added drop wise. The mixture was stirred at room temperature for 10 minutes and the resulting solution was allowed to slowly evaporate to give light pink crystals within 1-2 week (79% yield). M.p.>300 °C. Anal. Calcd for  $\text{C}_{23}\text{H}_{16}\text{N}_7\text{O}_{20}\text{Nd}$  (%): C, 32.01; H, 1.85; N, 11.46; Found: C, 32.14; H, 1.81; N, 11.30. IR ( $\text{cm}^{-1}$ ) selected bonds:  $\nu = 3589$  (b) (O-H), 3089 (m) (Ar-H), 1643(w) ( $\text{COO}^-$ )<sub>asy</sub>, 1539 (s) ( $\text{COO}^-$ )<sub>sy</sub>, 1410 (w) (C=C), 1348 (m) (N-O), 586 (w) (M-O).

### 1.3 Synthesis of $[\text{Nd}(\mu_2\text{-L2})(\text{L2})(\text{CH}_3\text{COO})(\text{H}_2\text{O})_2]_n$ (**2**)

To a solution of  $\text{Nd}(\text{CH}_3\text{COO})_3\cdot\text{H}_2\text{O}$  (0.339 g, 1 mmol) in 10 mL of water, 2-3 drops of NaOH 0.1 M were added. Then, a suspension of L2 (1 mmol, 0.21 g) in 20 mL of acetonitrile was added drop wise. The mixture was stirred for 10 minutes before transferring to a 40 mL Teflon-lined stainless steel vessel, which was sealed and heated at 120 °C for 24 h. After that the reaction system was slowly cooled to room temperature. Light Pink crystals were filtered off and dried in

air. (77% yield). M.p. >300 °C. Anal. Calcd for  $C_{16}H_{13}N_4O_{16}Nd$  (%): C, 29.03; H, 1.95; N, 8.46; Found: C, 29.05; H, 1.81; N, 8.30. IR ( $cm^{-1}$ ) selected bonds:  $\nu = 3578$  (b) (O-H), 3110 (m) (Ar-H), 1632 (s)  $(COO^-)_{asy}$ , 1536 (s)  $(COO^-)_{sy}$ , 1404 (m) (C=C), 1347 (m) (N-O), 592 (m) (M-O).

## 2. X-ray crystallography

X-ray data of compounds **1** and **2** were collected by CCD diffractometer and processed by SAINT. Lorentz and polarization effects and empirical absorption corrections were applied using SADABS from Bruker. The structures were solved by direct methods, using SIR-92<sup>1</sup> and refined by full-matrix least squares refinement methods<sup>2</sup> based on  $F^2$ , using SHELX-97. The hydrogen atoms of water molecules were located from the difference Fourier synthesis and were refined isotropically with distance of 0.82 Å with  $U_{iso}$  values 1.2 times that of their carrier oxygen atoms. All non-hydrogen atoms were refined anisotropically. All hydrogen atoms were fixed geometrically with their  $U_{iso}$  values 1.2 times of phenylene carbons and 1.5 times of terminal methyl carbons of acetonitrile solvent and acetate groups. All calculations were performed using Wingx package.<sup>3</sup> Crystal data as well as details of data collection and refinement for the complexes are summarized in Table S1.

## References

- (1) Altomare, A.; Cascarano, G.; Giacovazzo, C. ; Guagliardi, A. *J. Appl. Crystallogr.* **1993**, *26*, 343-350.
- (2) Sheldrick, G. M. *Acta Cryst A.* **2008**, *A64*, 112-122.
- (3) Farrugia, L. J. *J. Appl. Cryst.* **1999**, *32*, 837-838.

**Table S1.** Crystallographic data for compounds **1** and **2**.

Compound	<b>1</b>	<b>2</b>
Empirical formula	C <sub>23</sub> H <sub>16</sub> N <sub>7</sub> NdO <sub>20</sub>	C <sub>16</sub> H <sub>13</sub> N <sub>4</sub> NdO <sub>16</sub>
Formula weight	854.67	661.54
Temperature	296(2) K	296(2) K
Wavelength	0.71073 Å	0.71073 Å
Crystal system	Monoclinic	Monoclinic
Space group	P 2 <sub>1</sub> /n	P2 <sub>1</sub>
Unit cell dimensions	a = 9.4980(2) Å, α = 90°. b = 15.709(3) Å, β = 90.837(8)° c = 21.263(3) Å, γ = 90°.	a = 17.5380(5) Å, α = 90° b = 6.9480(2) Å, β = 101.684(12)° c = 19.1470(6) Å, γ = 90°
Volume	3172.19(10) Å <sup>3</sup>	2284.80(12) Å <sup>3</sup>
Z	4	4
Density (calculated)	1.790 Mg/m <sup>3</sup>	1.923 Mg/m <sup>3</sup>
Absorption coefficient	1.735 mm <sup>-1</sup>	2.362 mm <sup>-1</sup>
F(000)	1692	1300
Crystal size	0.12 x 0.08 x 0.05 mm <sup>3</sup>	0.11 x 0.08 x 0.06 mm <sup>3</sup>
Theta range for data collection	1.61 to 36.86°.	1.44 to 26.39°.
Index ranges	-16 ≤ h ≤ 10, -26 ≤ k ≤ 24, -35 ≤ l ≤ 35	-21 ≤ h ≤ 21, -8 ≤ k ≤ 8, -23 ≤ l ≤ 23
Reflections collected	62474	18573
Independent reflections	15887 [R(int) = 0.0358]	8187 [R(int) = 0.0251]
Completeness to theta	99.5 %	99.5 %
Absorption correction	Semi-empirical from equivalents	Semi-empirical from equivalents
Max. and min. transmission	0.7472 and 0.6299	0.7454 and 0.6179
Refinement method	Full-matrix least-squares on F <sup>2</sup>	Full-matrix least-squares on F <sup>2</sup>
Data / restraints / parameters	15887 / 4 / 473	8187 / 9 / 693
Goodness-of-fit on F <sup>2</sup>	1.022	0.702
Final R indices [I > 2σ(I)]	R1 = 0.0394, wR2 = 0.0748	R1 = 0.0233, wR2 = 0.0575
R indices (all data)	R1 = 0.0887, wR2 = 0.0900	R1 = 0.0255, wR2 = 0.0594
Largest diff. peak and hole	1.428 and -0.634 e.Å <sup>-3</sup>	0.798 and -0.451 e.Å <sup>-3</sup>
CCDC number	<b>1051022</b>	<b>1051023</b>

### 3. Results of X-ray crystallography

#### 3.1 $\{[\text{Nd}(\mu_2\text{-L1})_3(\text{H}_2\text{O})_2] \cdot \text{C}_2\text{H}_3\text{N}\}_n$ (**1**)

ORTEP of **1** is shown in Fig. S1. Each  $\text{Nd}^{\text{III}}$  ion in **1** has a bicapped trigonal prismatic geometry (Fig. S2(a)). The six sites are occupied by carboxylate oxygen atoms ( $\text{O13}^{\#1}$ ,  $\text{O14}$ ,  $\text{O15}^{\#2}$ ,  $\text{O16}$ ,  $\text{O17}^{\#1}$  and  $\text{O18}$  (#1:  $-x+1, -y, -z$ , #2:  $-x+2, -y, -z$ ) of **L1** and two sites by oxygen atoms ( $\text{O1W}$  and  $\text{O2W}$ ) of water molecules, forming twisted ribbons along  $a$  axis. Selected bond distances and angles are collected in Table S2.

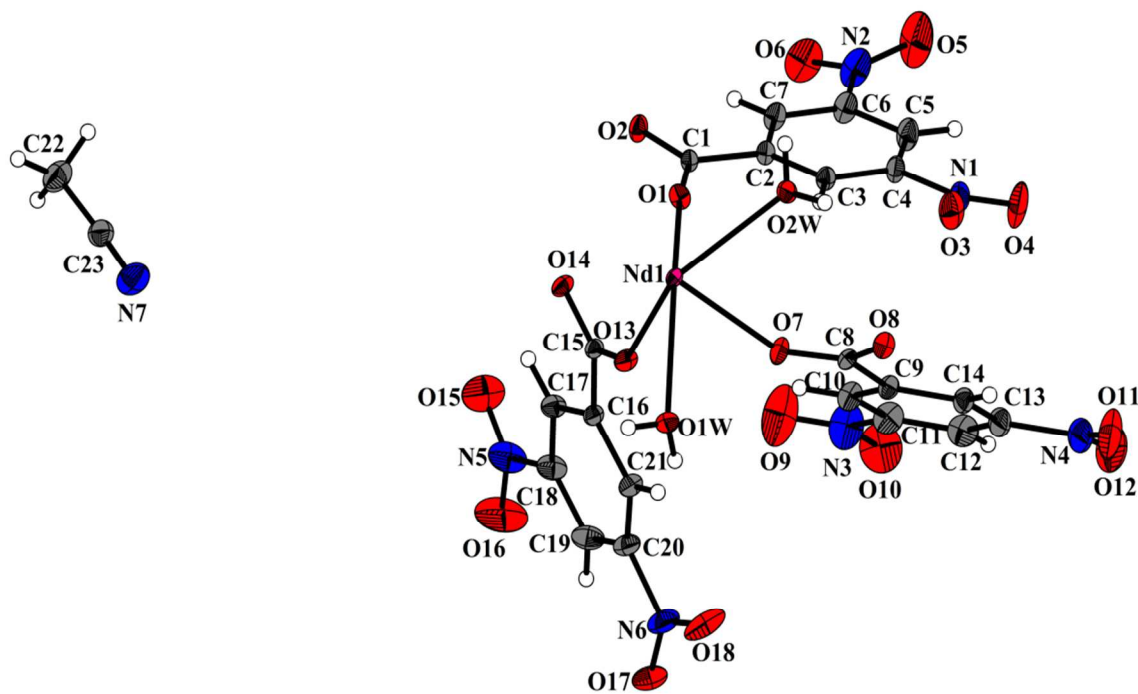


**Fig. S1.** ORTEP showing asymmetric unit of compound **1**, with 30 % probability.

**Table S2.** Selected bond lengths (Å) and angles (°) in compound **1**.

Nd(1)-O(1)	2.4186(16)
Nd(1)-O(7)	2.3840(18)
Nd(1)-O(13)	2.4534(17)
Nd(1)-O(1W)	2.6140(18)
Nd(1)-O(2W)	2.5199(18)
O(7)-Nd(1)-O(1)	90.61(7)
O(7)-Nd(1)-O(13)	76.50(6)
O(1)-Nd(1)-O(13)	74.18(6)
O(7)-Nd(1)-O(2W)	71.68(7)
O(1)-Nd(1)-O(2W)	74.63(6)
O(13)-Nd(1)-O(2W)	134.59(7)
O(7)-Nd(1)-O(1W)	70.24(7)
O(1)-Nd(1)-O(1W)	145.22(6)
O(13)-Nd(1)-O(1W)	73.24(6)
O(2W)-Nd(1)-O(1W)	122.50(6)

There are strong intramolecular H-bonding interactions between two coordinated water molecules (O1W and O2W) forming linear chain along *a* axis, further supporting the 1D CP (Fig. S2(b)). Additionally, O1W water molecule is also showing H-bonding with oxygens of –NO<sub>2</sub> groups in *bc* plane forming 2-D, H-bonded network (Fig. S2(c)). This creates 1D channels along *a* axis which are filled by acetonitrile molecules which are held by H-bonding of N7 with O2W water molecules (Fig. S2(d)) and aromatic C4 carbon atoms. The methyl hydrogens of acetonitrile are H-bonded to oxygens of nitro groups (Table S3).

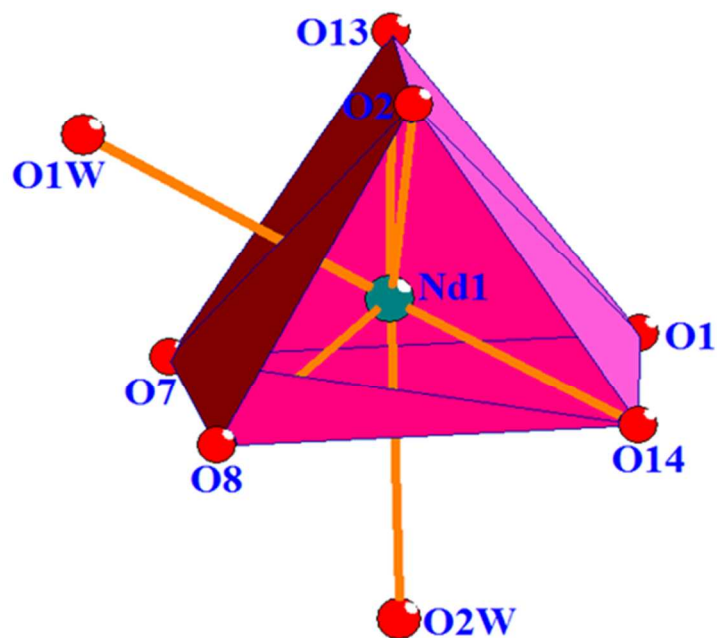


**Fig. S2 (a)** Trigonal bicapped geometry around  $\text{Nd}^{\text{III}}$  metal ion.

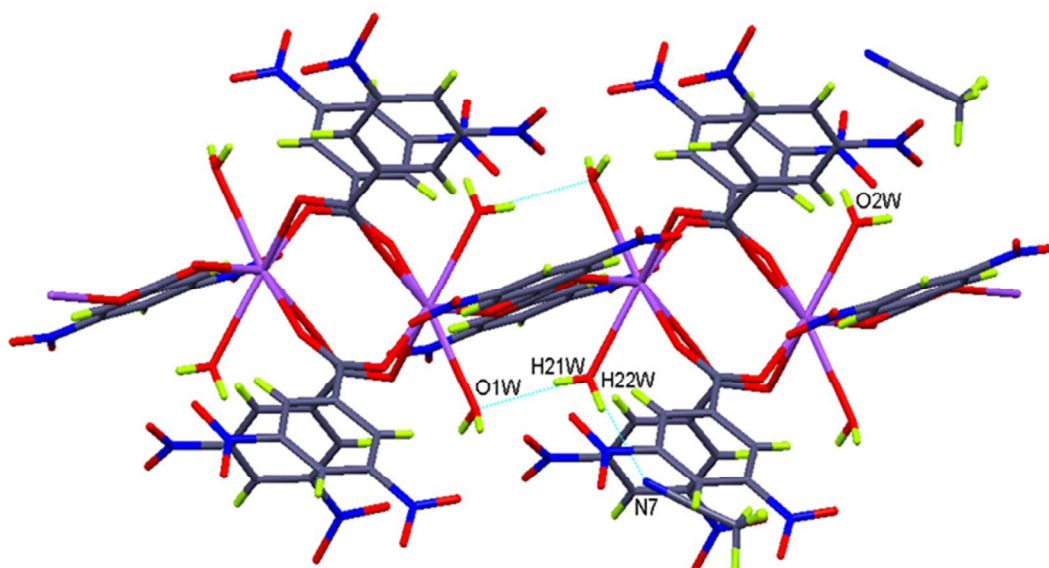


**Fig. S2 (b)** Coordination as well as H-bonded chain along *a* axis.

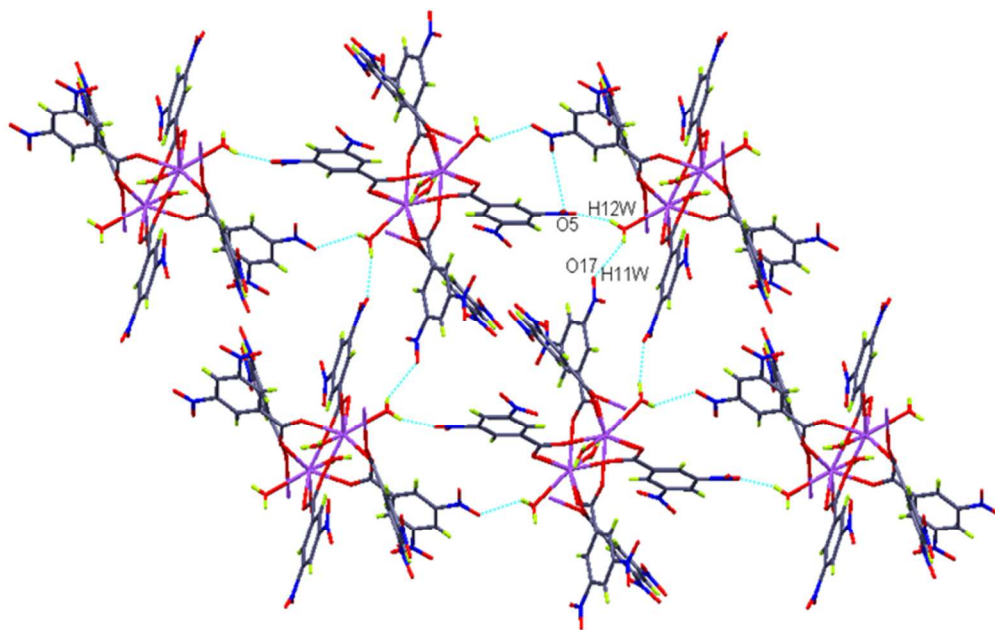


**Fig S2 (c)** 2D, H-bonded network between coordinated water O1W and oxygens of  $-\text{NO}_2$  groups in  $bc$  plane with channels along  $a$  axis.

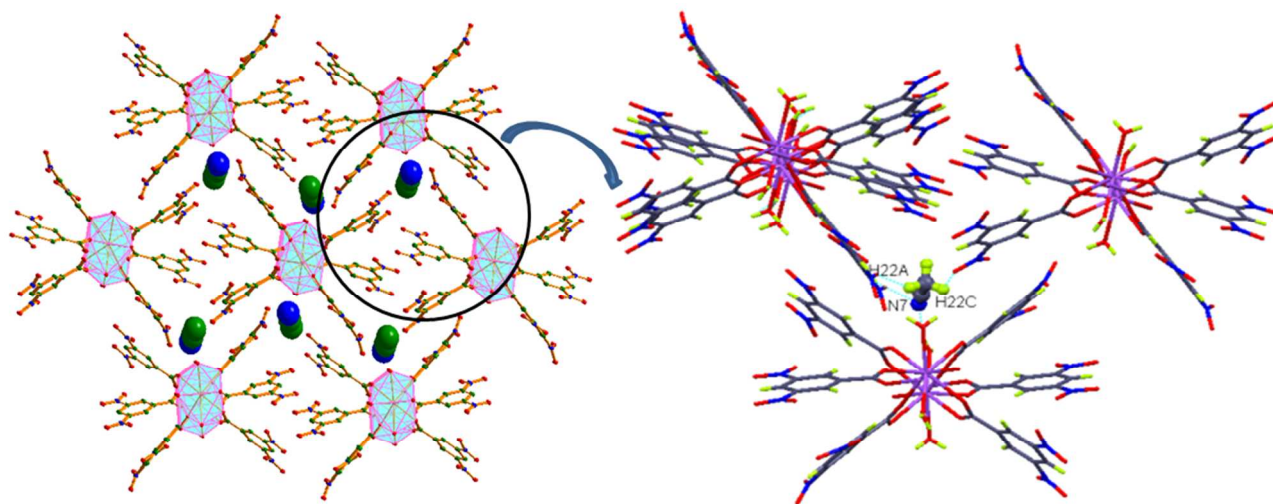


**Fig. S2 (d)** 2D H-bonded network with channels filled with acetonitrile molecules (expanded portion shows H-bonding interactions between solvent and the CP.)

**Table S3.** Hydrogen bond distances (Å) and angles (°) for compound **1**

X-H...Y	X...Y	H...Y	∠X-H...Y
O2W-H21W...O8	3.134(3)	2.65(3)	120
O1W-H11W...O2 <sup>1</sup>	2.794(3)	2.40(3)	111
C22-H22B...O11 <sup>1</sup>	3.542(6)	2.73	143
O1W-H12W...O6 <sup>2</sup>	3.488(4)	2.76(3)	153
O1W-H12W...O5 <sup>2</sup>	2.939(5)	2.24(3)	147
O1W-H12W...N2 <sup>2</sup>	3.564(4)	2.81(3)	158
O2W-H21W...O1W <sup>3</sup>	2.950(3)	2.15(2)	168
O1W-H11W...O3 <sup>3</sup>	3.359(4)	2.98(3)	111
O1W-H11W...O17 <sup>4</sup>	3.222(4)	2.57(3)	139
O2W-H22W...N7 <sup>5</sup>	2.809(4)	2.04(3)	159
O2W-H22W...O5 <sup>6</sup>	3.416(5)	2.96(3)	119
C22-H22A...O6 <sup>7</sup>	3.407(5)	2.57	146
C22-H22B...O16 <sup>8</sup>	3.223(6)	2.76	111
C22-H22C...O2 <sup>9</sup>	3.681(5)	2.99	132
C22-H22C...O17 <sup>10</sup>	3.204(5)	2.67	115
C22-H22C...O18 <sup>10</sup>	3.470(5)	2.81	126

(1) -x+1,-y,-z (2) x+1/2,-y-1/2,+z+1/2 (3) -x+2,-y,-z (4) -x+1/2+1,+y+1/2,-z+1/2

(5) x+1/2,-y+1/2,+z-1/2 (6) -x+1/2+1,+y+1/2,-z-1/2 (7) -x,-y,-z (8) x,+y+1,+z

(9) x-1,+y+1,+z (10) x-1/2,-y+1/2,+z+1/2

### 3.2 $[\text{Nd}(\mu_2\text{-L2})(\text{L2})(\text{CH}_3\text{COO})(\text{H}_2\text{O})_2]_n$ (**2**)

ORTEP of **2** is shown in Fig. S3. Selected bond length and angles are collected in Table S4.

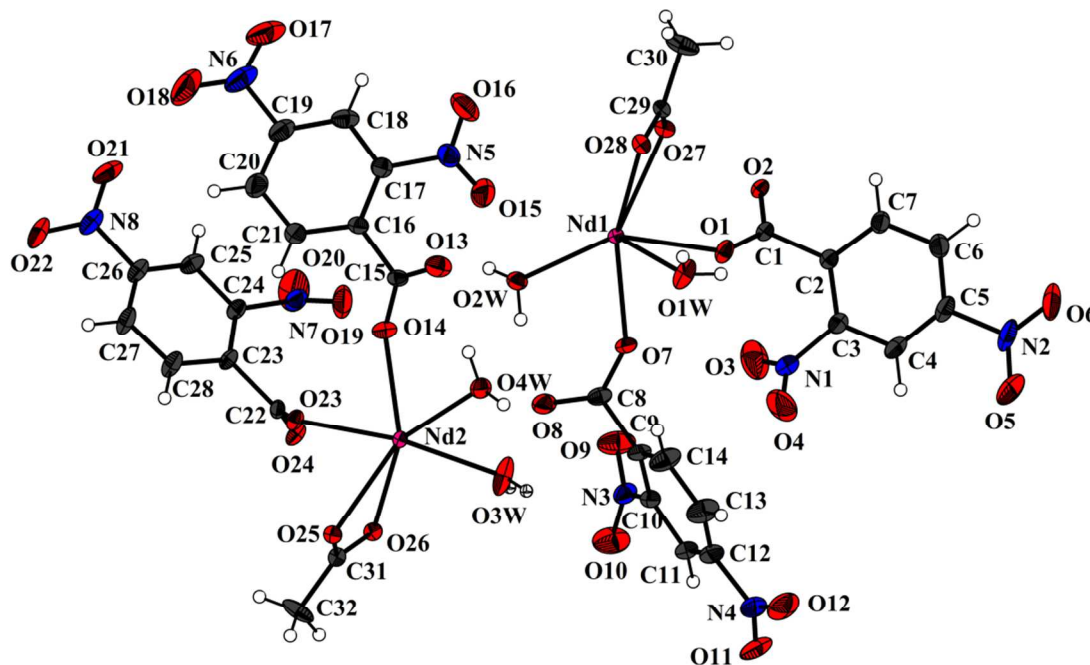


**Fig. S3.** ORTEP showing asymmetric unit of compound **2**, with 30 % probability

**Table S4.** Selected bond lengths (Å) and angles (°) in compound **2**.

O(1)-Nd(1)	2.470(3)	O(7)-Nd(1)-O(2W)	69.78(11)
O(1W)-Nd(1)	2.469(4)	O(7)-Nd(1)-O(1W)	71.85(14)
O(2W)-Nd(1)	2.460(3)	O(2W)-Nd(1)-O(1W)	126.82(14)
O(3W)-Nd(2)	2.501(4)	O(7)-Nd(1)-O(1)	75.11(13)
O(4W)-Nd(2)	2.421(3)	O(2W)-Nd(1)-O(1)	133.25(13)
O(7)-Nd(1)	2.400(3)	O(1W)-Nd(1)-O(1)	65.81(11)
O(14)-Nd(2)	2.404(3)	O(7)-Nd(1)-O(27)	145.91(14)
O(23)-Nd(2)	2.518(3)	O(2W)-Nd(1)-O(27)	131.18(11)
O(25)-Nd(2)	2.536(3)	O(1W)-Nd(1)-O(27)	100.86(13)
O(26)-Nd(2)	2.629(3)	O(1)-Nd(1)-O(27)	71.71(12)
O(27)-Nd(1)	2.591(3)	O(7)-Nd(1)-O(28)	142.80(13)
O(28)-Nd(1)	2.625(3)	O(2W)-Nd(1)-O(28)	131.66(11)
		O(1W)-Nd(1)-O(28)	71.38(12)
		O(1)-Nd(1)-O(28)	94.82(12)
		O(27)-Nd(1)-O(28)	49.46(9)
		O(14)-Nd(2)-O(4W)	69.07(12)
		O(14)-Nd(2)-O(3W)	115.76(16)
		O(4W)-Nd(2)-O(3W)	70.82(14)
		O(14)-Nd(2)-O(23)	72.89(11)
		O(4W)-Nd(2)-O(23)	140.89(11)
		O(3W)-Nd(2)-O(23)	136.86(12)
		O(14)-Nd(2)-O(25)	135.90(12)
		O(4W)-Nd(2)-O(25)	135.42(13)
		O(3W)-Nd(2)-O(25)	107.83(15)
		O(23)-Nd(2)-O(25)	71.02(11)
		O(14)-Nd(2)-O(26)	135.63(11)
		O(4W)-Nd(2)-O(26)	145.94(12)
		O(3W)-Nd(2)-O(26)	76.11(13)
		O(23)-Nd(2)-O(26)	71.53(10)
		O(25)-Nd(2)-O(26)	49.73(10)

There are two crystallographically independent molecules present in the unit cell of compound **2**. The geometry around Nd<sup>III</sup> ion is tricapped trigonal prismatic (Fig. S4(a)) by coordinating with **L2** to form 1D coordination polymer along *b* axis (Fig. S4(b)). In each one of crystallographically independent chains, intramolecular H-bonding interactions among coordinated water molecules, methyl groups, aromatic rings and –COO, –NO<sub>2</sub> groups, further support the propagation of 1D CP along *b* axis (Fig. S4(c)). Two crystallographic independent 1D chains, in turn are connected to each other through intermolecular H-bonding interactions involving coordinated waters and oxygens of –COO and –NO<sub>2</sub> groups (Fig. S4(d)). These interactions lead to form a 2D network, further extending in *bc* plane, having various supramolecular synthons like **R<sub>4</sub><sup>2</sup>(8)**, **R<sub>1</sub><sup>1</sup>(6)**, **R<sub>2</sub><sup>1</sup>(6)**, **R<sub>1</sub><sup>2</sup>(7)** and **R<sub>1</sub><sup>2</sup>(4)** (Fig. S4(e)). Weak H-bonding interactions between –NO<sub>2</sub> groups and protons of aromatic rings extend the network to 3D as shown in *ac* plane (Fig. S4(f) (Table S5)).

The coordination number of Nd<sup>III</sup> ion, coordination modes of ligand, Point symbol and topology, dimensionality, M···M distances and chirality of compounds **1** and **2** are listed in Table S7.

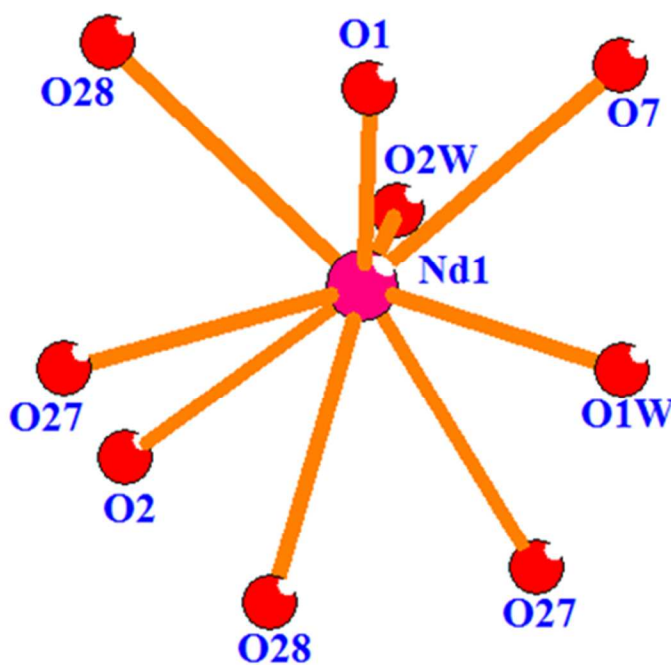


**Fig. S4 (a)** Trigonal prismatic tricapped geometry around Nd<sup>III</sup> metal ion.

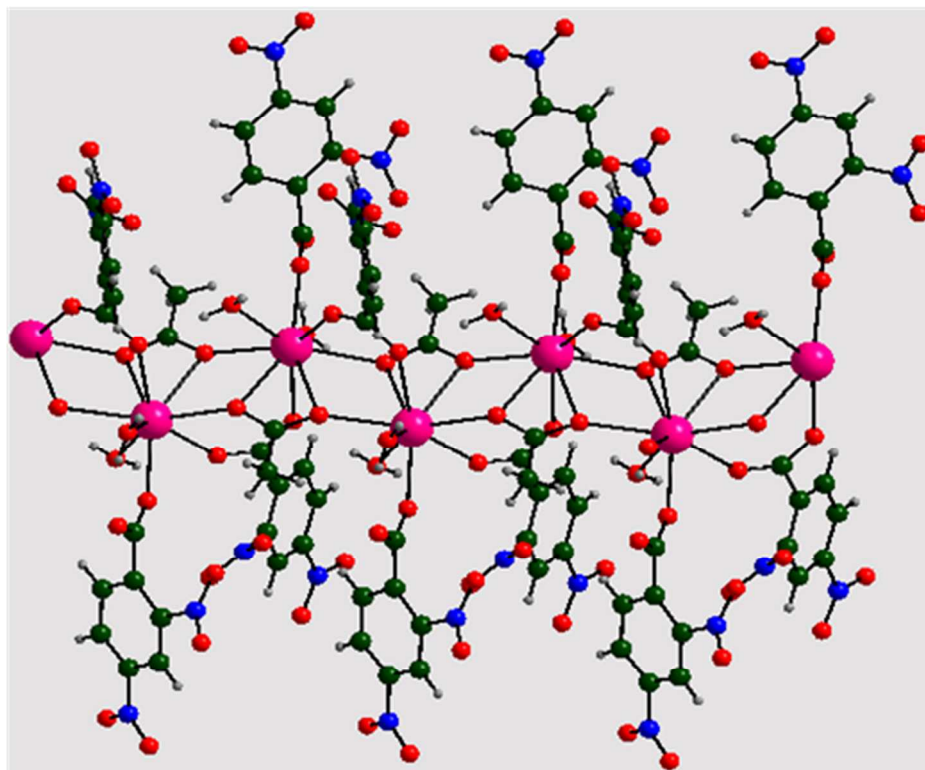


**Fig. S4 (b)** Molecular structure of 1-D polymeric compound (**2**) along *b* axis (only one crystallographically independent chain is shown).

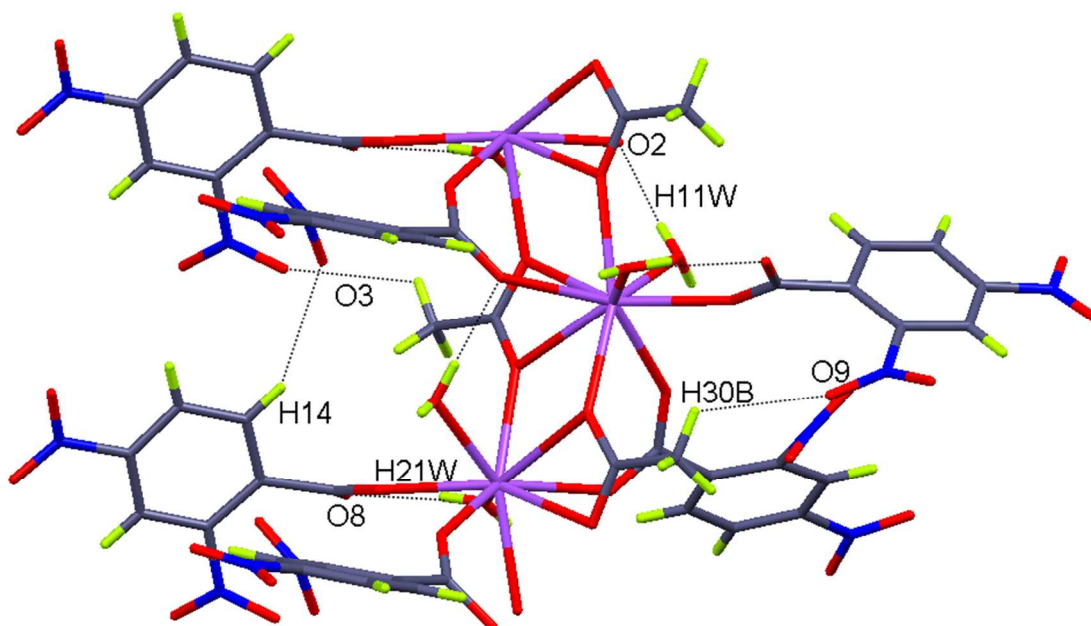


**Fig. S4 (c)** Intramolecular H-bonding interactions among coordinated water molecule,  $-\text{COO}$ ,  $-\text{NO}_2$  groups, protons of methyl group and aromatic ring. (only one crystallographically independent chain is shown).

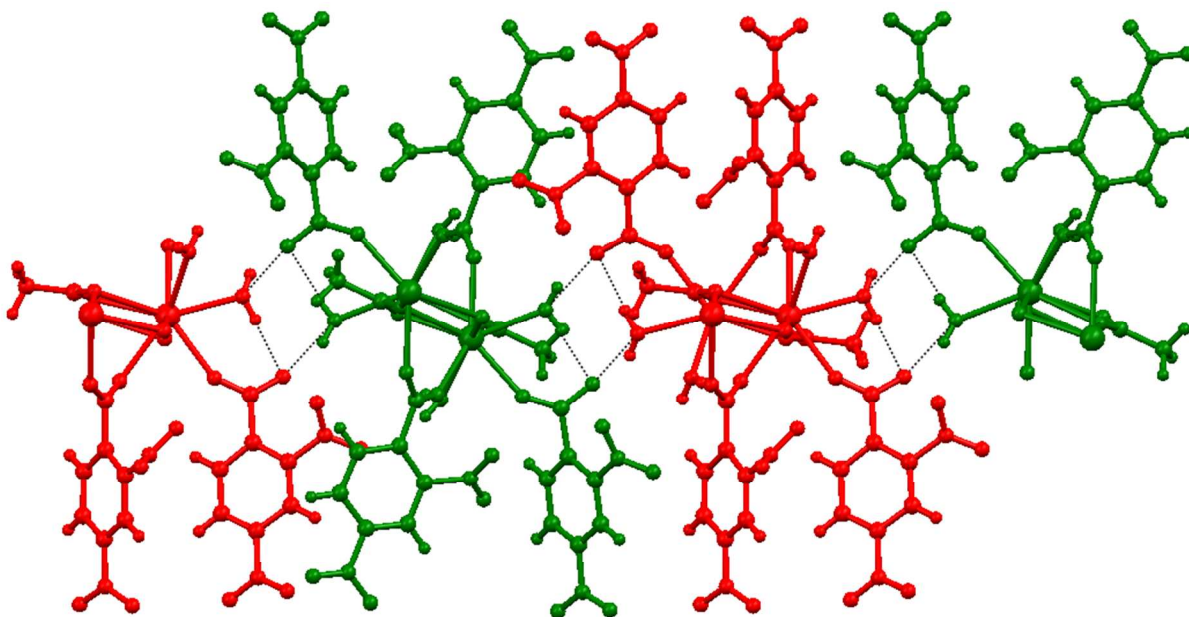


**Fig. S4 (d)** H-bonding interactions between two crystallographic independent 1D chains (red and green color) extending the network further in *bc* plane.

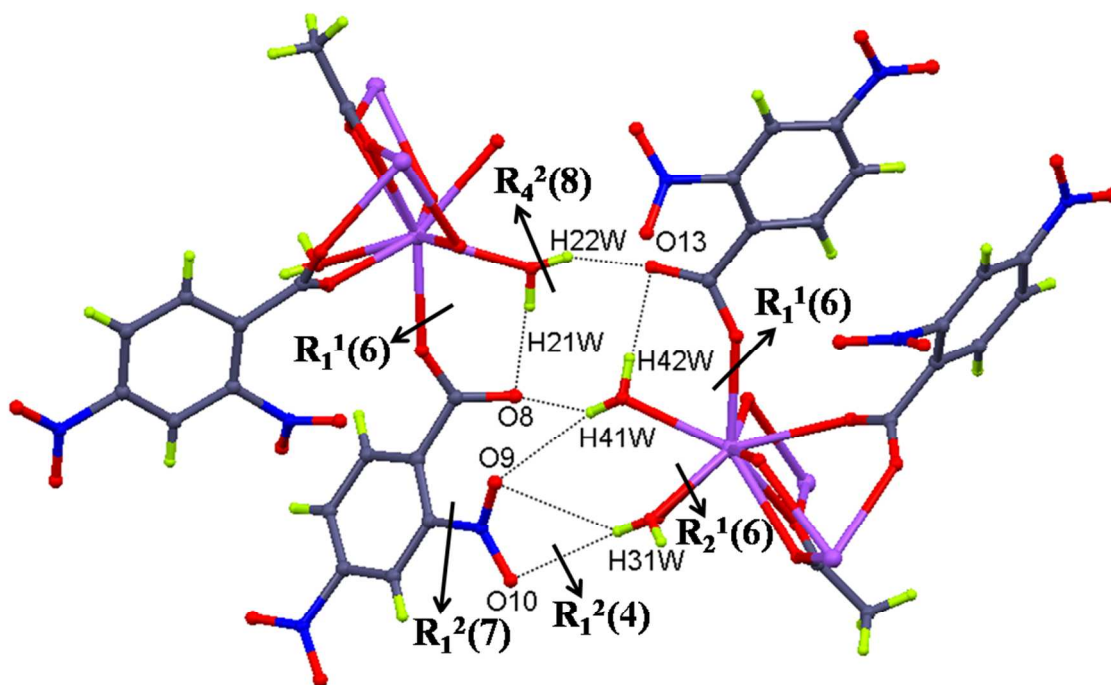


**Fig. S4 (e)** Zoomed in H-bonded area from Fig. S4(d) to show H-bonding interactions between two crystallographic independent chains forming various supramolecular synthons.

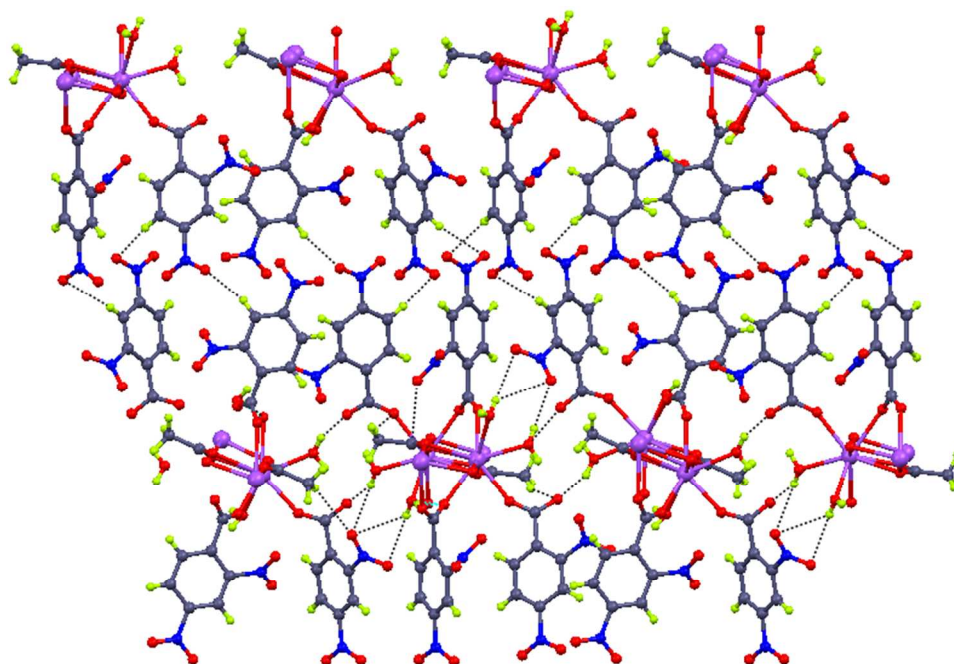


**Fig. S4 (f)** Weak H-bonding interactions between  $-\text{NO}_2$  groups and protons of aromatic rings forming 3D network (shown in *ac* plane).

**Table S5.** Hydrogen bond distances ( $\text{\AA}$ ) and angles ( $^\circ$ ) for compound **2**

$\text{X-H}\cdots\text{Y}$	$\text{X}\cdots\text{Y}$	$\text{H}\cdots\text{Y}$	$\angle\text{X-H}\cdots\text{Y}$
O2W-H21W $\cdots$ O4W	3.360(5)	2.93(5)	115
O2W-H21W $\cdots$ O7	2.781(4)	2.39(4)	110
O2W-H21W $\cdots$ O8	2.720(4)	1.91(3)	169
O2W-H22W $\cdots$ O13	2.833(6)	2.08(5)	153
O3W-H31W $\cdots$ N3	3.721(7)	2.96(6)	158
O3W-H31W $\cdots$ O9	3.322(7)	2.71(7)	134
O3W-H31W $\cdots$ O10	3.383(7)	2.58(5)	172
O4W-H41W $\cdots$ O8	2.733(6)	2.00(6)	149
O4W-H41W $\cdots$ O9	3.167(6)	2.63(5)	125
O4W-H42W $\cdots$ O2W	3.360(5)	2.89(6)	118
O4W-H42W $\cdots$ O13	2.781(5)	1.96(4)	172
O4W-H42W $\cdots$ O14	2.736(5)	2.31(5)	113
O1W-H11W $\cdots$ O2 <sup>1</sup>	2.725(5)	1.94(5)	162

O3W-H32W...O23 <sup>2</sup>	2.737(6)	1.94(5)	161
C32-H32C...O8 <sup>2</sup>	3.699(8)	2.78	160
C32-H32B...O13 <sup>2</sup>	3.521(8)	2.65	151
C32-H32A...O14 <sup>3</sup>	3.474(8)	2.63	146
C32-H32A...O15 <sup>3</sup>	3.479(7)	2.82	126
C30-H30B...O4W <sup>4</sup>	3.567(8)	2.99	120
C30-H30B...O7 <sup>4</sup>	3.761(9)	2.92	147
C30-H30B...O9 <sup>4</sup>	3.245(7)	2.69	117

(1)  $x, +y+1, +z$  (2)  $-x+1, +y-1/2, -z+2$  (3)  $-x+1, +y+1/2, -z+2$  (4)  $-x+1, +y+1/2, -z+1$

#### 4. Thermo gravimetric analysis

Thermal decomposition of these compounds were carried out under nitrogen at heating range of 10 deg min<sup>-1</sup>. The TGA curve of **(1)** (Fig. S5a) shows that at 109 °C temperature, the loss of 5.8 % (calcd 4.8 %) weight due to loss of acetonitrile solvent molecule from lattice (wt left 94.2%, calcd 95.2 %) with endothermic peak of -2.25 W/g. After that at 320 °C, loss of coordinated water molecules is taking place (wt 90.78 %, calcd 90.99 %) and endothermic peak is observed of -2.51 W/g. The complex is stable up to 406 °C and decomposition of the parent complex, with explosion and a sharp exothermic peak of 3.31 W/g, is observed at 409 °C.

Compound **2** (Fig. S5b) is stable up to 68 °C, after that it loses 5.44 % weight of two coordinated water molecules (weight left 95.49 %, calcd 95.67 %) and at 215 °C it loses 8.9 % weight due to one acetate anion (weight left 84.34 %, calcd 84.37 %), beyond that it is stable up to 244 °C where it finally decomposes with explosion giving a sharp exothermic peak of 0.343 W/g.

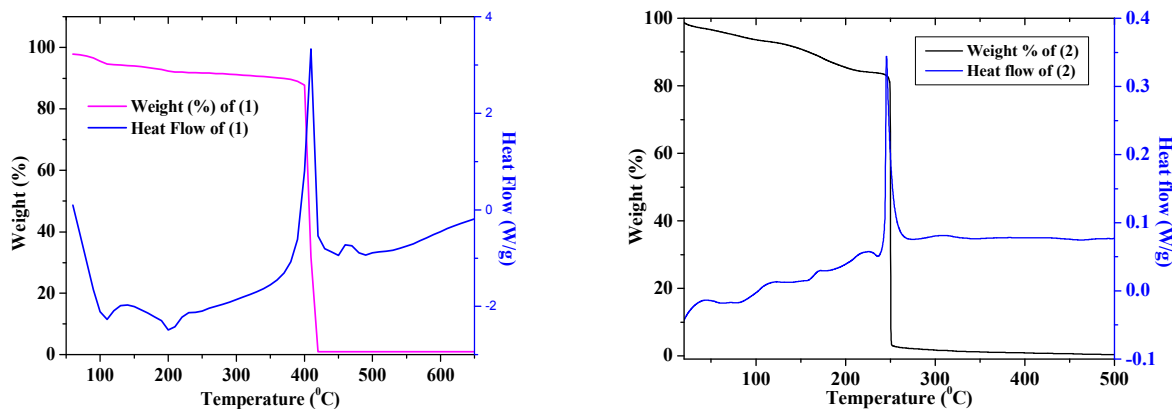


Fig. S5. TGA graph of (a) compound 1 and (b) compound 2.

### 5. IR spectroscopy

In both complexes of  $\text{Nd}^{\text{III}}$  ions, symmetric and anti symmetric  $-\text{OH}$  stretching bands appears as broad bands in the region of  $3575\text{--}3589\text{ cm}^{-1}$ . The C-H and C-C vibrations belonging to the aromatic rings are found around  $3082\text{--}3112\text{ cm}^{-1}$  and  $1404\text{--}1412\text{ cm}^{-1}$ . The characteristic peaks of asymmetric and symmetric stretches of  $\text{COO}^-$  are found in the regions  $1630\text{--}1643\text{ cm}^{-1}$  and  $1535\text{--}1539\text{ cm}^{-1}$  respectively. The complexes contain aromatic N-O stretch in the region of  $1346\text{--}1349\text{ cm}^{-1}$  and weak bands around  $583\text{--}592\text{ cm}^{-1}$  are assigned to M-O vibrations (Fig. S6, Table S6).

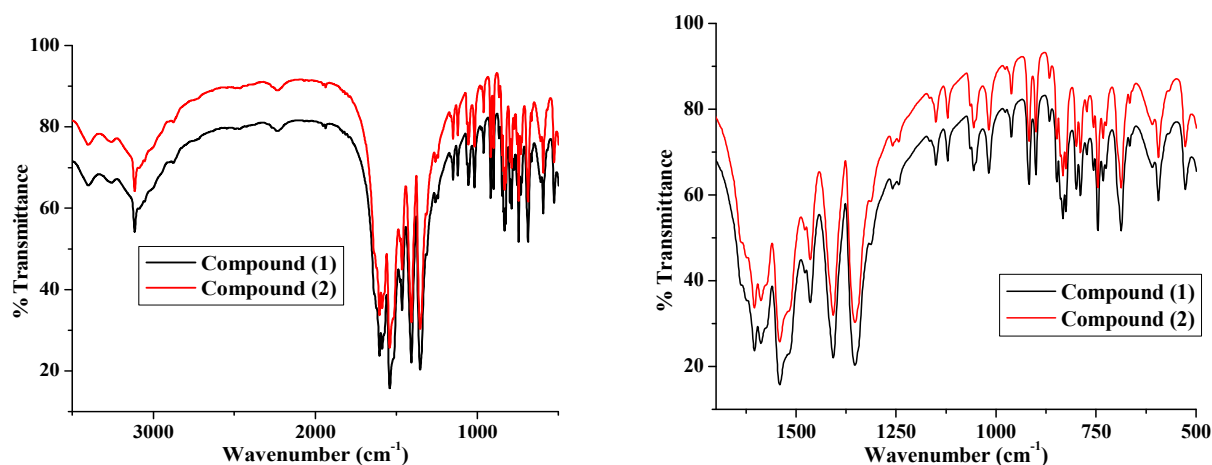


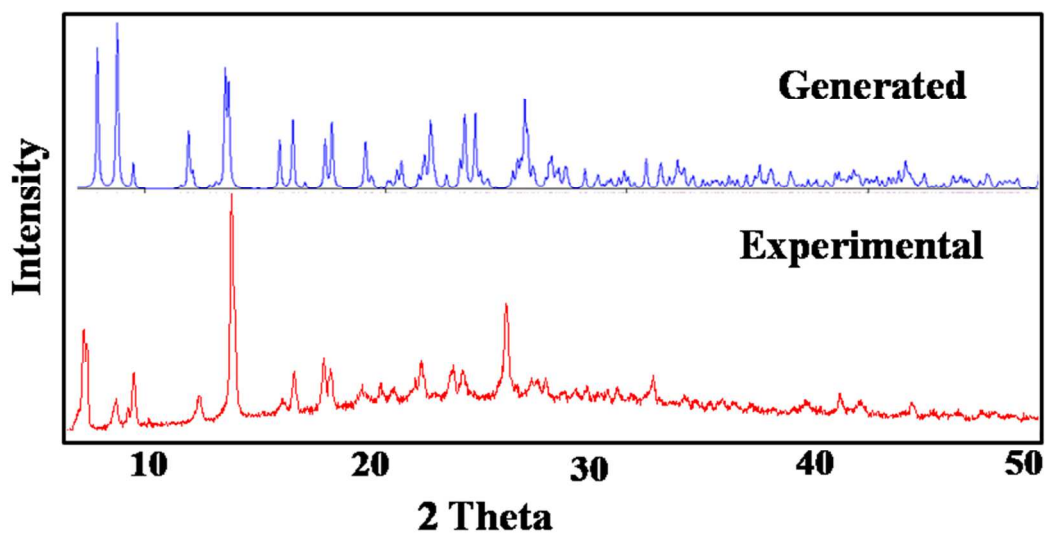
Fig. S6. IR spectra of compounds (1) and (2).

**Table S6.** IR frequencies of main functional groups

Code	O-H	(COO <sup>-</sup> ) <sub>asy</sub>	(COO <sup>-</sup> ) <sub>sy</sub>	N-O	M-O
1	3589	1643	1539	1348	586
2	3578	1632	1536	1347	592

## 6. PXRD studies

The PXRD patterns of compounds (1) and (2) are similar to the simulated ones from their crystal structure (Fig. S7 and S8) indicating the homogeneity of the samples.

**Fig. S7.** Showing generated and experimental PXRD patterns of compound (1)

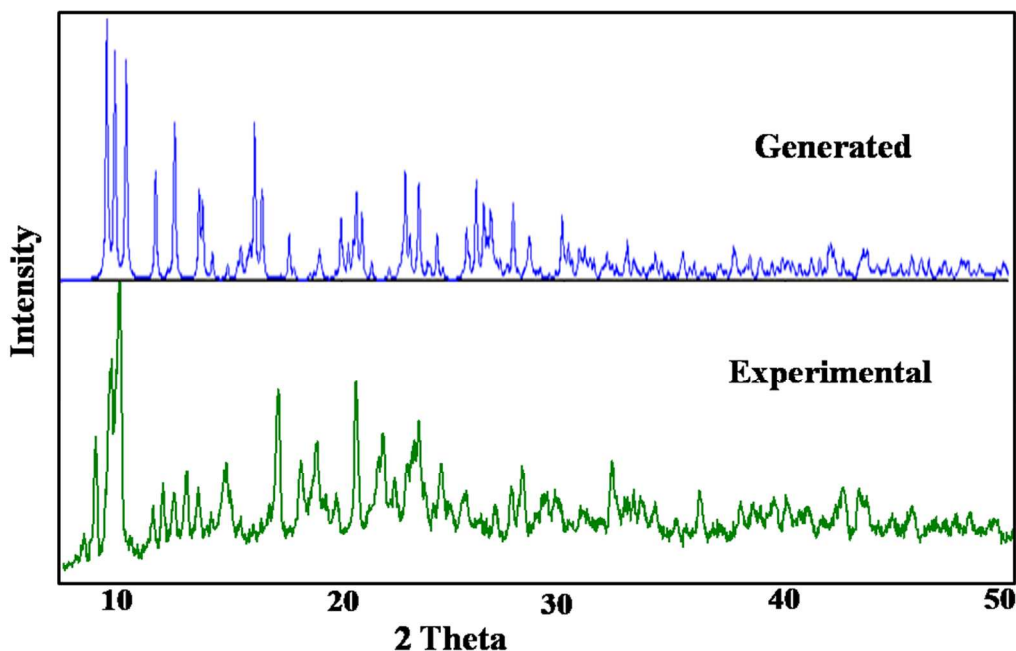
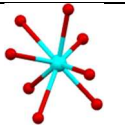
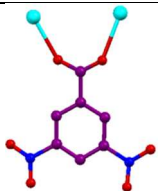
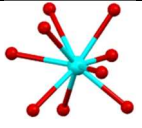
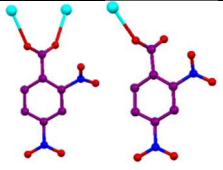
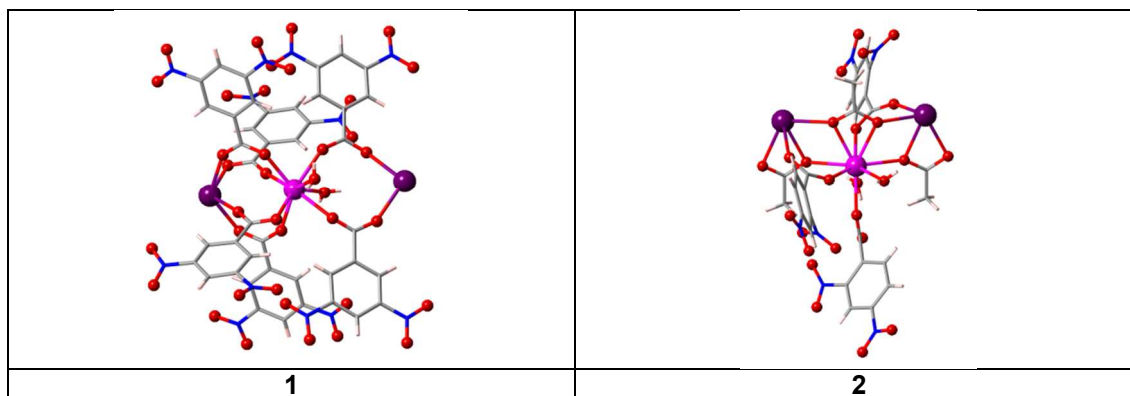


Fig. S8. Showing generated and experimental PXRD patterns of compound (2)

Table S7. Coordination numbers of Nd<sup>III</sup> ion, coordination modes of ligand, Point symbol and topology, dimensionality, M···M distances and chirality of compounds 1 and 2.

Compound	Coordination no. of Nd <sup>III</sup> ion	Coordination mode of ligand	Point Symbol and topology	Loss of solvents, Decomposition temperature (D)	M···M distance (Å)	Chirality
1			[1 0 0] chains with 2-c uninodal net	109 °C - loss of one lattice acetonitrile solvent, 320 °C-loss of coordinated water, 414 °C-D	4.267, 5.348	-
2			{3 <sup>3</sup> .4 <sup>2</sup> .5}, [0 1 0] chains, 4-c uninodal SP1-periodic net	68 °C - loss of two coordinated water, 215 °C-loss of acetate anion, 244 °C-D	4.221	Chiral

## 7. Magnetic study



**Fig. S9.** Truncated models for **1** and **2**. Color code: Nd, magenta; La, purple; O, red; N, blue; H, white.

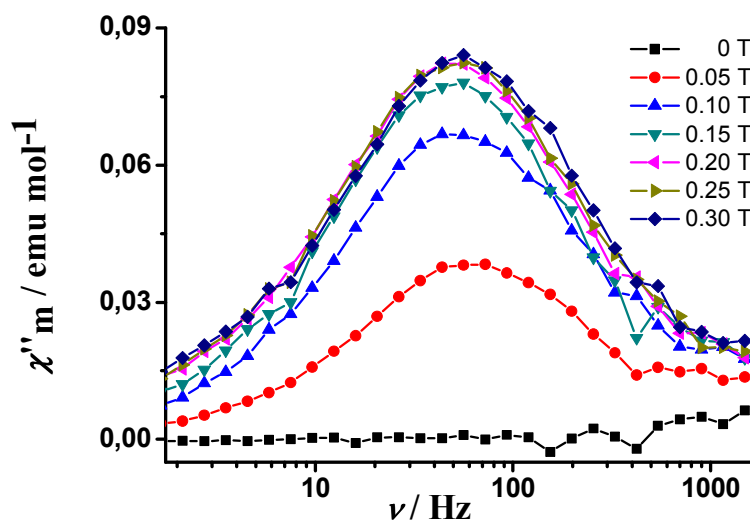


**Fig. S10.** Frequency dependence of the out-of-phase molar susceptibility ( $\chi''_m$ ) signal at 2 K with applied fields in the 0-0.3 T range for compound **1**.

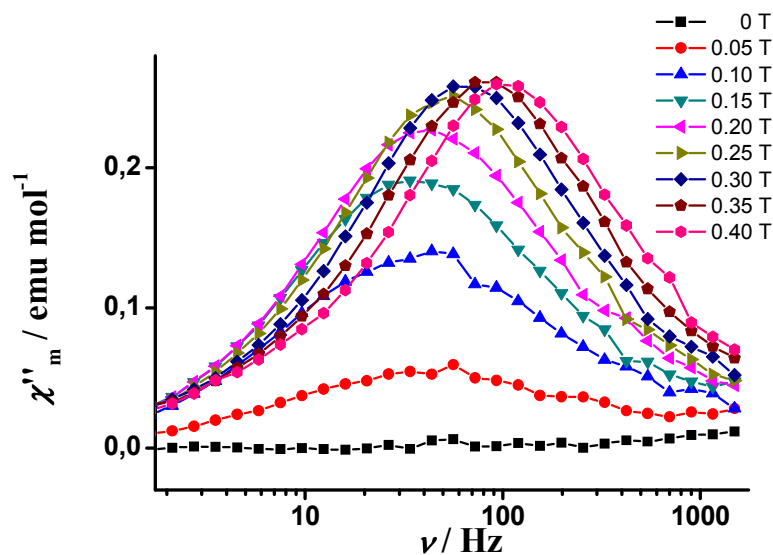


**Fig. S11.** Frequency dependence of the out-of-phase molar susceptibility ( $\chi''_m$ ) signal at 2 K with applied fields in the 0-0.4 T range for compound **2**.

List of frequencies used in the study of the ac frequency-dependence of compounds (**1**) and (**2**) in Fig. 3 (Manuscript):

1488.095, 1284.247, 1102.941, 946.9657, 822.3684, 704.8872, 608.7662, 523.743, 450.7212, 389.0042, 334.8214, 288.4615, 248.6737, 214.0411, 184.5472, 159.1681, 137.0614, 118.0731, 101.6811, 87.61682, 75.48309, 65.01387, 56.00359, 48.25013, 41.57428, 35.80978, 30.85912, 26.58066, 22.89936, 19.72853, 17.00834, 14.64844, 12.61437, 10.87083, 9.36002, 8.06521, 6.95062, 5.98506, 5.1579, 4.44229, 3.82715, 3.29734, 2.84091, 2.44753, 2.10845, 1.81658, 1.5648, 1.34884, 1.16073, 1.00058 Hz.